Ref. Ares(2019)6678754 - 29/10/2019

Horizon 2020
European Union Funding
for Research & Innovation

DELIVERABLE D3.2

REPORT SUMMARISING THE LITERATURE REVIEW

for Selection of Representative Syngas Compositions including Organic and Inorganic Contaminants

DISSEMINATION LEVEL: PUBLIC

Grant Agreement (GA) N. 85284

Research and Innovation Actions (RIA) project

Granted by:

Innovation and Networks Executive Agency (INEA)

Document Control Sheet

Project	**BLAZE** - Biomass Low cost Advanced Zero Emission small-to-medium scale integrated gasifier-fuel cell combined heat and power plant
Grant Agreement n.	85284
Document Title	Deliverable D3.2 “Report summarising the literature review” for Selection of Representative Syngas Compositions including Organic and Inorganic Contaminants
Lead Beneficiary	P N° 3 – SOLIDpower S.A.
WP number	WP3
Type	Report
Dissemination level	Public

Version	Date	Description
v1	25.4.2019	First draft prepared by author
v1	9.5.2019	Feedback from Andrea di Carlo
v2	25.6.2019	Second draft prepared by author
v2	4.7.2019	Feedback from Andrea di Carlo and Luca Del Zotto
v2	26.8.2019	Deliverable revised by USGM (Enrico Bocci)
v3	12.09.2019	Final version drafted by the author

Date	12/09/2019
Number of pages	32
Archive name	D3.2
Authors	J.P. Ouweltjes (SOLIDpower S.A.)
Contributors	A. Di Carlo (Università de L’Aquila)
Reviewer(s)	E. Bocci, L. Del Zotto (USGM)

This project has received funding from the European Union’s Horizon 2020 research and innovation programme under grant agreement No 815284

TABLE OF CONTENT

LIST OF FIGURES

LIST OF TABLES

This project has received funding from the European Union's Horizon 2020 research and innovation programme under grant agreement No 815284

1 EXECUTIVE SUMMARY

Within the BLAZE project, an SOFC from SOLIDpower will be integrated with a bubbled fluidised bed steam gasifier developed by UNIVAQ, USGM and WALTER TOSTO. This report has been made in order to understand if there are potential risks if the producer gas is fed to the SOFC. After an introduction in chapter 2, the current level of understanding what will be the gas quality, considering both relatively clean biomass feedstock (e.g. almond shells) and relatively dirty biodegradable waste (e.g. municipal solid waste) are considered and will be given in chapter 3. Then, chapter 4 summarises in a broad sense what is known about the operation of SOFCs with carbonaceous gases as well as the impact of contaminants that might exist in bio-syngas arriving from a BFB steam gasifier. Chapter 5 concludes with giving recommendations about the experiments that need to be carried out in work package 3 in order to successfully demonstrate the integrated system in WP 6.

This deliverable is related to milestone MS3 "Selection of the test conditions for the experimental work"

The indicators of success are the identification of at least 5 experimental and 5 simulative international peer reviewed papers on gasifiers/hot gas conditioning systems in order to select at least 2 representative compositions and 2 organic and 3 inorganic representative contaminants levels. This report identified 83 papers (mostly experimental) instead of 10, and 1 representative composition (owing to the decision to focus only on the steam gasification tested at pilot scale) and 2 organic (toluene and naphthalene) and 3 inorganic (H2S, KCl; HCl) representative contaminants levels.

2 INTRODUCTION

2.1 Objectives and scope of the document

Directive (EU) 2018/2001 on the promotion of the use of energy from renewable sources states that biomass refers to "the biodegradable fraction of products, waste and residues from agriculture (including vegetal and animal substances), forestry and related industries, as well as the biodegradable fraction of industrial and municipal waste". According to this definition, biomass resources include a wide range of materials, e.g. wood chips, straw, miscanthus, poultry waste, sewage sludge, etc., which have diverse physical and chemical properties.

Three conversion processes can be employed to produce fuel gas from biomass:

- Anaerobic digestion, which is the conversion of biomass to primarily methane (CH_4) and carbon dioxide (CO_2) by micro-organisms in the absence of oxygen (typically between 10°C and 60°C).
- Pyrolysis, which is the thermal decomposition (typically above 300 °C) of biomass in the absence of oxygen. The major products are char, bio-oil and gas that mainly contains CH_4, CO_2, carbon monoxide (CO) and hydrogen (H_2).
- Gasification, which is the thermal decomposition (typically above 650 °C) of biomass in the presence of gasification agents, e.g. air, oxygen, steam, CO_2 or a combination of them that transforms the biomass into so-called bio-syngas that contains CO, H_2, CH_4, steam, CO_2, light hydrocarbons and, in case of air gasification, nitrogen (N_2). The fuel gas may contain a certain amount of impurities, e.g. tar, particulate matter, char, hydrogen sulfide (H_2S) and/or hydrogen chloride (HCl).

Among these three conversion processes, gasification is an interesting option for integration with fuel cells in order to produce electric power. Especially bubbling fluidized bed (BFB) steam gasifiers have proven to produce relatively clean fuel with high calorific value. On the fuel cell side, solid oxide fuel cells (SOFCs) are an interesting candidate due to their high operating temperature between 650 and 1000^{o}C, especially when intermediate cooling is avoided. It is for this reason that this combination will be investigated within the BLAZE project.

Although SOFCs are relatively fuel tolerant, it is unlikely that integration of a BFB steam gasifier and an SOFC is possible without additional gas conditioning and gas cleaning. Deep understanding about the impact of the fuel main constituents and fuel contaminants on the SOFC performance is thus required. This literature review provides an overview of what is currently known about the potential issues that bio-syngas might have on the SOFC longevity, and will give the necessary guidelines for the tests performed within in WP2 (gasifier operating conditions and hot gas conditioning) and those performed within WP3 (SOFC single cell tests and short stack tests) in order to make the final demonstration in

WP6 successful.

2.2 Structure of the deliverable

As an introduction to the main part of this deliverable where the operation of SOFCs with bio-syngas is discussed, chapter 3 provides an introduction to the characteristics of bio-syngas obtained by BFB steam gasifiers. Chapter 4 then provides a broad review of what is currently known about operating SOFCs with carbonaceous fuels, including their tolerance for organic and inorganic contaminants. Chapter 5 concludes this report by summarising the main outcomes from chapter 4 in relation to the fuel expected from a BFB steam gasifier, followed by giving recommendations for the experimental work that will be considered in BLAZE work package 3.

3 BIO-SYNGAS SPECIFICATION

With respect to the gasifier that is considered for integration with an SOFC in the BLAZE project, there is a recent publication that mentions about the gas quality, either without additional gas cleaning as well as after gas cleaning with catalytic filters. The experimental work focused on evaluating a commercially available catalytic filter under three test conditions, i-empty candle, ii-candle partially filled with catalyst pellets and iii-candle totally filled with catalyst pellets. The composition of the main reactants in the gas while operating the gasifier at 1053 or 1093 K is shown in Figure 1 [Savuto, 2019]. In comparison to the ideal gas composition predicted by thermodynamic calculations, the results in the test with the empty candle show a lower H_2 content and H_2O conversion, while the CH_4 content was higher than expected. On the other hand, the results obtained with the partially filled candle are close to the theoretical thermodynamic values, implying that the catalyst promotes the steam reforming of hydrocarbons.

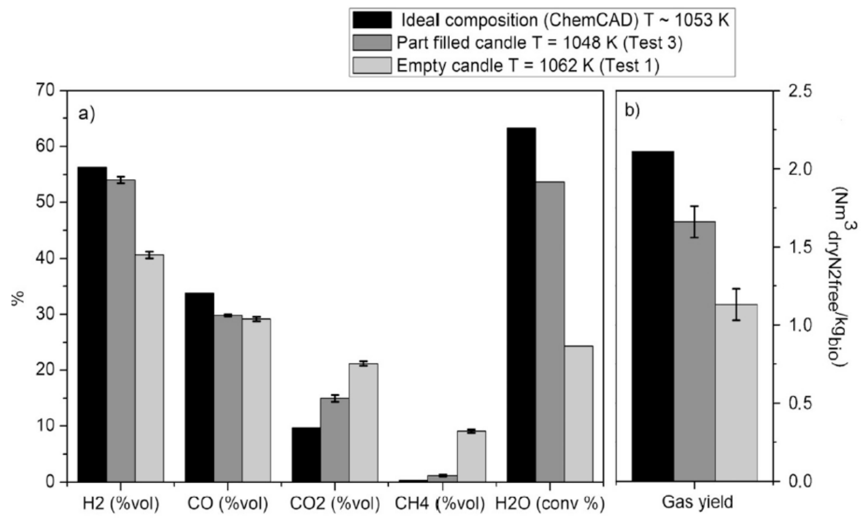

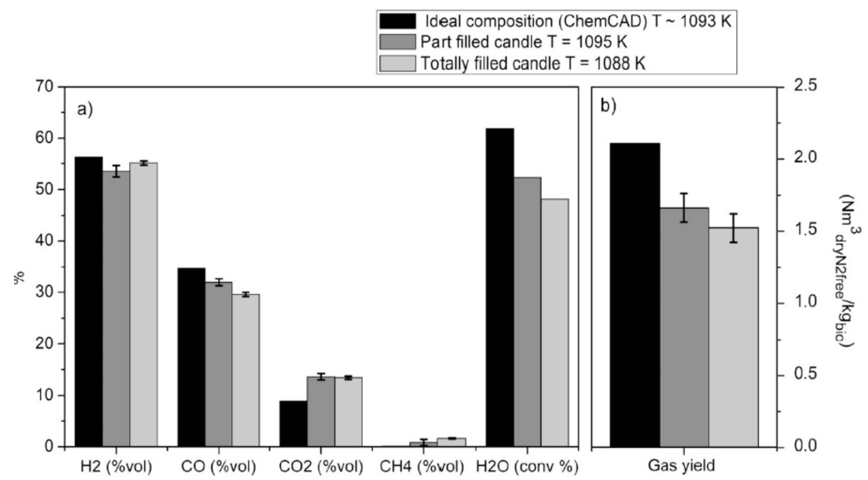

Figure 1. Gas composition obtained with a bench scale BFB steam gasifier [Savuto, 2019].

This project has received funding from the European Union's Horizon 2020 research and innovation programme under grant agreement No 815284

Besides particulates, tars belong to the major contaminants generated during the gasification of biomass. Their formation is related to two different pathways: 1) the direct release of aromatic structures in lignin devolatilization, and 2) a mechanism of hydrogen abstraction and acetylene addition [Rakesh, 2018]. According to Kinoshita et al. [Kinoshita, 1994], tar yield and tar concentration decrease as the equivalence ratio increases as more oxygen is available to react with volatiles in the flaming pyrolysis zone. They also reported that the residence time has little influence on the tar yield, but that it influences the tar composition, where the amounts of oxygen-containing compounds tend to decrease with increasing residence time, resulting in a decreasing yield of 1- and 2-ring compounds (except benzene and naphthalene) while the amount of 3-ring and 4-ring compounds increases. The main species of tar that are generated during the gasification thus range from single to five-ring type of aromatic hydrocarbons. These constituents can reside in the hot gas stream as vaporised material or as persistent aerosols. But usually they condense at lower temperatures.

Table 1 summarizes the results from the tar analyses that were carried out on the bench-scale BFB steam gasification tests using olivine sand as the bed material and almond shells as biomass feedstock, performed by Savuto et al [Savuto, 2019].Considering tests from 2-1 to 3-3, it can be seen that the catalytic filter caused a considerable reduction in tar concentration. The total tar concentration (including benzene) dropped from 5.8 g/Nm^3 to 0.4 g/Nm^3 (average value). The cleaned tar consisted of 1-ring compounds (predominantly toluene), the two-ring compound naphthalene (on average 37 mg/Nm^3, or 7 ppm), and to a small extent higher-ring tars. A further reduction of the tar concentrations, which will be investigated within the BLAZE project, is expected to come from the addition of dolomite to the olivine [Rapagnà, 2018; Pallozzi, 2018]. On the other hand, it should be noted that tar yields in the gasification of almond shells are relatively low. When municipal solid waste is gasified, the tar concentrations are typically 1 to 2 times higher than in the case of just wood [Wilk, 2013; Campoy, 2014].

	TAR + benzene (mg/Nm^3)							
	Test 1	Test 2-1	Test 2-2	Test 2-3	Test 3-1	Test 3-2	Test 3-3	Test 4
Benzene	2439	130	157	111	75	70	78	–
1-Ring compounds	1711	230	193	199	230	266	230	189
Naphthalene	616	51	16	7	13	113	25	62
2-Ring compounds	479	~0	~0	2	~0	10	3	80
3- and 4-ring compounds	470	49	9	6	78	56	46	57
Phenols	0	0	0	0	0	0	0	0
Total Tar	3276	330	218	214	321	445	304	388
Tar + benzene	5715	460	375	325	396	515	382	–

Table 1. Tar analysis performed during the gasification experiments by Savuto et al. [Savuto, 2019]. Test from 2-1 to 3-3 were performed with candle partially filled with catalyst pellets. Test from 2-1 to 2-3 and from 3-1 to 3-3 were performed at 820°C and 775°C respectively.

Furthermore, several experimental tests in fluidized bed gasifiers at laboratory and industrial scale demonstrated that ceramic candles, with the addition of Ni catalyst, are able to completely remove particulate by means of their anisotropic porous filtering structure, and furthermore efficiently reduce tar (< 200 mg/Nm3 [D'Orazio 2015, Rapagnà 2010-2012, Nacken 2015]).

Besides tars, the producer gas will contain particulate matter (PM), sulphur compounds, hydrogen chloride, alkali metal species and nitrogen compounds, especially ammonia. It is assumed that catalytic filters that will be considered in the BLAZE project for hot gas conditioning will remove most of the particulate matter, and will bring down PM concentrations below 1 mg/Nm^3 [Heidenreich, 2013]. For high temperature applications like SOFC, the removal of the other contaminants at high temperatures is favourable. Alkali vapors are condensed below 500-700°C forming particles (< 5 micron) to combine with tars. At higher temperatures, they can be removed by hot adsorption onto solid sorbents. For HCl removal, alkali metal compounds could be injected into the gasifier which results in forming salts that can be filtered in the same way as particulate matter. Nitrogen compounds can be removed by e.g. thermal catalytic decomposition. They have proven to be easily converted in SOFCs and are therefore not considered to be detrimental. For further information about hot gas cleaning in a broad sense, the reader is kindly referred to the relevant literature. Excellent reviews were made by e.g. Ud Din [Ud Din, 2016] and Aravind [Aravind, 2012]. For hot gas cleaning relevant for the integrated system considered in BLAZE, further information can be found in a publication from Stemmler et al. [Stemmler, 2013 (1)]. Based on thermodynamic calculations, considering the BFB steam gasifier in Guessing which is similar to the gasifier used in BLAZE, contaminant levels before hot gas cleaning and after hot gas cleaning are reported for many inorganic contaminants, see Figure 2.

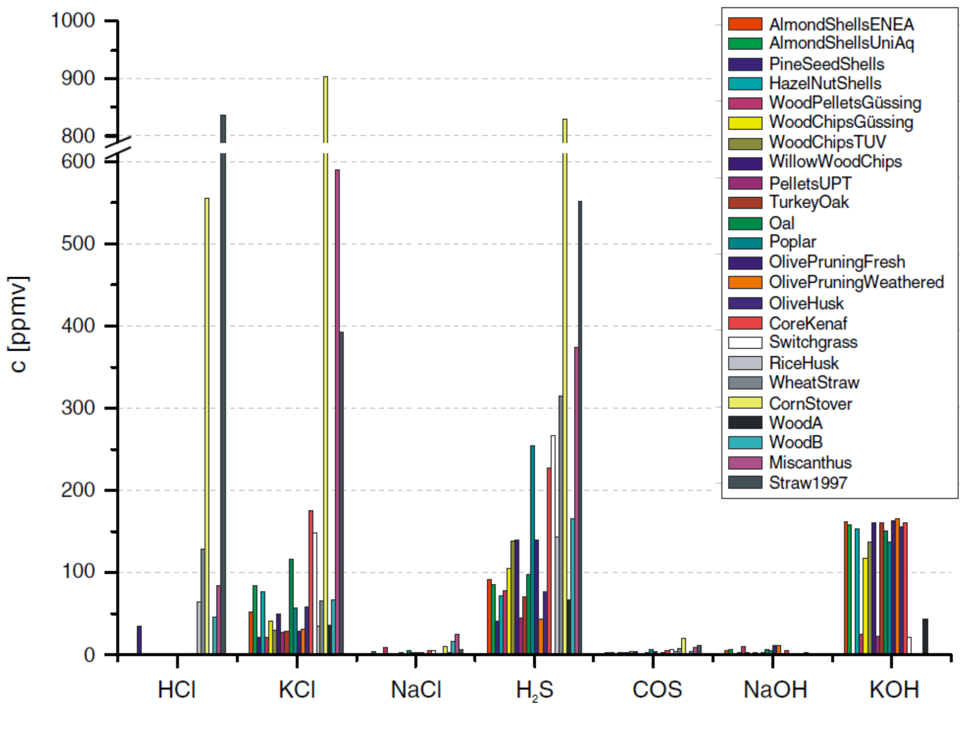

Figure 2. Predicted inorganic contaminants levels before hot gas cleaning [Stemmler, 2013 (1)].

This project has received funding from the European Union's Horizon 2020 research and innovation programme under grant agreement No 815284

Based on the above results reported by Stemmler, and those reported by Canova and Bushnell for refuse-derived fuel (RDF) from municipal solid waste [Canova, 1993], which is considered to contain the highest contaminant levels, the following ranges for inorganic contaminants are given in Table 2. Like for the tars, it is expected that these contaminant levels can be brought down by using improved hot gas cleaning. For the removal, promising results have been obtained by using aluminosilicate [Stemmler, 2013 (2)], and thus the use of this material will be addressed in WP2. In Stemmler 2013 (2) bauxite, bentonite, kaolinite and the natural occurring zeolite were investigated as sorbent for high temperature removal of KCl, using a gas stream laden with 20 ppmv KCl. The results of the KCl sorption experiments show that bauxite, kaolinite and natural occurring zeolite are suitable sorbents for KCl removal below 100 ppbv at 800–900 °C at least during the first hours of the experiments. However, kaolinite was the only sorbent that kept the 100 ppbv limit longer than 50 h.

Compound	Almond shells	RDF
(K+Na)Cl	50-80	400-900
(K+Na)OH	150-200	50
H_2S	80-100	800-900
HCl	0	550-850

Table 2. Contaminant levels for almond shells and refuse-derived fuel (RDF) prior to hot gas cleaning

This project has received funding from the European Union's Horizon 2020 research and innovation programme under grant agreement No 815284

4 OPERATING SOFCs WITH CARBONACEOUS FUELS

4.1 Generic considerations

Hydrocarbons can be directly utilised in solid oxide fuel cells by internal reforming, either with steam or with CO_2 that are added to the fuel, or that may form while the fuel cell is under electrical load. This has become clear from the abundant experimental results reported in literature, which show that, for example, operation with methane is possible at a steam to carbon (S/C) ratio of 1.5-1.6, while higher S/C ratios are needed to convert higher hydrocarbons [Mogensen, 2011]. Although the addition of steam to the fuel may be beneficial for the prevention of catalytic carbon deposits, this is somewhat undesirable in fuel cell operation, as addition of steam to the anode side of the cell reduces the electrical potential according to the Nernst equation. In order to know if carbon deposits due to catalytic reactions are preferentially formed, it is thus helpful to reveal the extent of carbon deposition in a C-H-O ternary diagram. Once the ratio among these three components is determined, it will become clear if carbon formation is significant by assuming complete equilibriums between the fuel constituents. At 1000°C, no carbon deposition is expected if the carbon-to-oxygen ratio is less than unity. With decreasing temperature, it can be found that the deposition region expands deeply into the carbon poor region if we consider thermodynamic equilibrium [Alstrup, 1998]. Operation without the formation of detrimental amounts of solid carbon then relies on slow formation kinetics and/or rapid solid carbon removal kinetics, as will be shown below.

4.2 The risk of carbon deposition

Some researchers have reported results about the operation of SOFC anodes under dry or slightly humidified hydrocarbon fuel, thus relying on the removal of carbon adspecies by oxygen ions pumped through the electrolyte. Mechanistic studies were performed by Horita et al. who investigated the catalytic methane decomposition on well-defined model anodes [Horita, 2004 (1); Horita, 2004 (2)]. For stripe-shaped Ni films on yttria stabilized zirconia (YSZ) and yttria doped ceria (YDC), the amount of carbon deposited on the Ni surface on YDC was smaller than that on YSZ, which the authors ascribed to the ability of YDC to affect the distribution of hydrogen, carbon and oxygen atoms around the Ni/YDC interface. It was suggested that when water vapor adsorbs on the nickel surface, it is dissociated and hydrogen is transported to the Ni/YDC interface. And since protons can be dissolved in YDC, the transported hydrogen can be ionized as protons in YDC. The proton can then react with oxygen ions to form H_2O, and this is evaporated as steam around the surface of YDC. This reaction may enhance the adsorption of steam on the nickel surface, which eventually increases the concentration of water on the nickel surface and eventually helps to react with carbon adspecies which can then desorb from the nickel surface. Likewise, the conductivity properties of YSZ don’t allow for the formation of steam, and

This project has received funding from the European Union’s Horizon 2020 research and innovation programme under grant agreement No 815284

thus makes Ni-YSZ more prone to carbon deposition. Later, it was reported by Yamaji et al. that the properties of the support influence the nature of the deposited carbon upon exposure to methane. The results indicated that graphite-like carbon is mainly formed on Ni films on YSZ and ScSZ, while the amount of amorphous-like carbon is relatively high on GDC and LSGM [Yamaji, 2008]. The influence of electrochemically produced steam was reported by Lin et al. [Lin, 2006], who showed that stable operation with Ni-YSZ in dry methane was possible, but only at a current density of 1.8 Acm^{-2}, which is far higher than a typical current density for commercial SOFC systems. Below that, the cells degraded rapidly, revealing severe coking upon dismounting.

The conversion of other hydrocarbons supplied in high concentrations to SOFCs have been experimentally investigated as well. In a comparative study, Yamaji et al. reported about the operation of Ni-ScSZ anode under ethane with low steam concentrations. From their results it followed that ethane is prone to thermal cracking upon introducing the fuel at the fuel inlet port. Upon arrival at the anode, the cracked ethane was observed to be removed by electrochemically produced H_2O or CO_2, which was evidenced by a decrease near the anode/electrolyte interface [Yamaji, 2006]. A year later, it followed by a comparative study by this group on the operation of Ni-ScSZ anode under methane, ethane and propane that the larger the hydrocarbon molecule, the higher the risk of carbon formation due to cracking. It was thus suggested and evidenced that in order to suppress carbon deposition, the SOFC operating temperature should be reduced to slow down the kinetics for hydrocarbon cracking, even while the fuel utilization should be kept high in order to produce sufficient H_2O and CO_2 to remove deposited carbon. Similarly, Saunders et al. observed only small amounts of carbon deposits when a polarised Ni-YSZ anode was injected with methanol or methanoic acid, where less carbon was found as the temperature increased, while rapid cell deactivation took place when the anode was fed with ethanol, ethanoic acid, butanoic acid, or n-octane. In the case of n-octane, little carbon was found at 700°C while severe coking occurred at 800°C [Saunders, 2004]. Kishimoto et al. have reported about Ni-ScSZ operation with n-dodecane at 800°C. Also in this case, severe carbon deposition took place at the fuel entry, while the anode itself was basically free of carbon, which made the authors to suggest that steam produced by the SOFC helped to remove deposited carbon [Kishimoto, 2004]. They later showed that the addition of steam to n-dodecane up to a S/C ratio of 2 allowed for operation under carbon free conditions at 800°C and 55% fuel utilization [Kishimoto, 2007]. Kim et al. operated Ni-YSZ anodes with toluene at 700°C and experienced severe carbon deposition and cell failure [Kim, 2001]. Timmermann et al. investigated unpolarised Ni-YSZ anode between 650 and 850°C in syngas including up to 0.5% acetylene and found that carbon deposition became more problematic at lower operating temperature [Timmermann, 2007]. Despite the fact that the amount of carbon that was formed at 650°C was lower than would follow from thermodynamic calculations, it shows that carbon deposition from hydrocarbons at SOFC relevant operating conditions is a tedious problem and that the real solution to mitigating carbon deposition is to look for operating conditions where kinetics are sufficiently fast while thermodynamics do not give rise to carbon formation (in this case 850^{o}C with less than 0.1% acetylene).

From the above literature it follows that besides carbon deposits formed via reactions over the anode catalyst, pyrolytic carbon may be formed via free-radical gas-phase condensation reactions. It is the result of C-C bond scission at high temperatures [Baker, 1975 (1); Baker, 1975 (2); Keep, 1977; Baker, 1989, Monnerat, 2001; Toh, 2003]. This phenomenon originates from free radical gas phase reactions, which are favoured at high temperatures and are supposed to have a high affinity for the formation of higher hydrocarbons that may deposit in the anode as pyrolytic carbon (also called amorphous char). In the case of carbon deposition from methane (or any other combustible molecule including only one carbon atom), it is most likely the surface reaction with the catalyst that causes carbon, as C-H bonds are much stronger than the C-C bonds in higher hydrocarbons that could lead to pyrolytic carbon [Mermelstein, 2009].

Carbon deposition and carbon formation in the SOFC anode may have detrimental consequences for the anode microstructure. When hydrocarbons adsorb on a Ni catalyst they are dehydrogenated, leading to atomic carbon and hydrogen. Depending on the other surface ad-atoms, the atomic carbon might react, e.g. with oxygen, in order to form a desorbable product or other intermediates. Atomic carbon itself is not stable on the surface and if it doesn't react with any other ad-species it may give rise to the formation of carbon clusters, where graphitic carbon may lead to the formation of encapsulating carbon, causing catalyst deactivation, or the formation of carbon whiskers/fibers/filaments/nanotubes. Their typical hollow nature is thought to be related to concentration gradients of carbon along the nickel particle due to super-saturation on the catalyst-gas interface with respect to graphite saturation [Holstein, 1995]. After reaching a sufficiently high carbon concentration in the nickel particle, carbon precipitation at the catalyst-support interface may occur (Figure 2). This mechanism implies that it may depend on the nickel particle size and shape before a critical carbon concentration is reached and the growth of carbon filaments starts to occur.

This project has received funding from the European Union's Horizon 2020 research and innovation programme under grant agreement No 815284

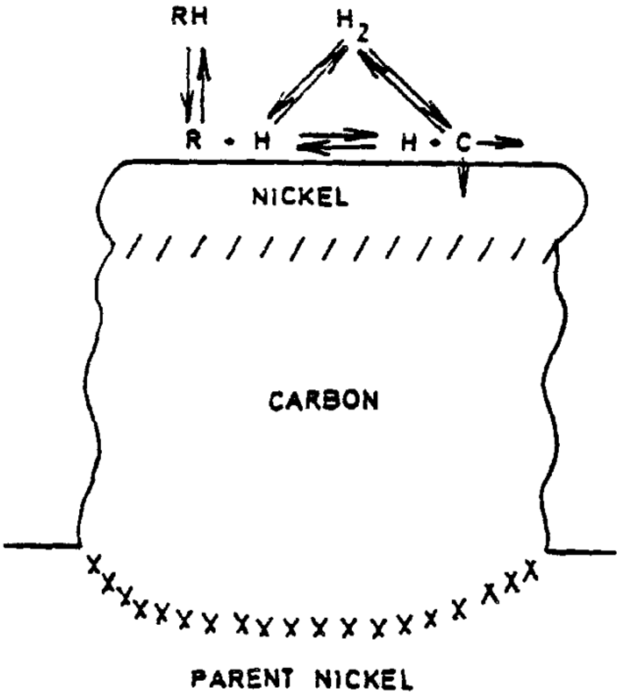

Figure 3. Carbon precipitation at the catalyst-support interface .

Likewise, the formation of graphite on the nickel surface may result in disintegration of the metal, and hence this process is known as metal dusting. Nickel is known for its strong activity for CO dissociation with, due to the low stability of nickel carbide, direct graphitization as a result. Polished nickel surface exposed to CO-H_2 mixture with 1% steam at 680°C were reported to possess areas with a uniform graphite layer penetrating the metal as tongue-shaped intrusions, while many fine nickel particles (5 to 20 nm in diameter) were observed in the coke layer. Also, some large nickel particles had been detached from the metal surface by the graphite penetration. Authors thus concluded that the tongue-shaped intrusions were the main culprits for nickel dusting [Young, 2009]. It was further suggested by Szakalos that initially, larger metal fragments may be released from the metal dusting front. These larger metal pieces are subjected to continued fragmentation until they finally may be too small for inward growth of graphite or graphite nucleation in their interior and the continued formation of solid carbon will occur on their surface [Szakalos, 2004].

4.3 Exposure to tars

Similar to lower hydrocarbons like alkanes, tars can decompose due to reforming reactions, cracking and solid carbon formation. The following overall reactions are important for the conversion of tar species [Devi, 2005; Nguyen, 2016; Trimm 1977]:

This project has received funding from the European Union's Horizon 2020 research and innovation programme under grant agreement No 815284

Steam reforming:

$$C_nH_m + n\,H_2O \rightarrow C_{n'}\,H_{m'} + \left(n+\frac{m}{2}\right)H_2 + n\,CO \quad (1)$$

$$\text{Dry reforming: } C_nH_m + n\,CO_2 \rightarrow \left(\frac{m}{2}\right)H_2 + 2n\,CO \quad (2)$$

$$\text{Hydro cracking: } C_nH_m + H_2 \rightarrow C_{n'}H_{m'} \quad (3)$$

$$\text{Thermal cracking: } C_nH_m \rightarrow C_{n'}H_{m'} + H_2 \quad (4)$$

$$\text{Carbon formation: } C_nH_m \rightarrow n\,C + \left(\frac{m}{2}\right)H_2 \quad (5)$$

$$\text{Water-gas shift: } CO + H_2O \rightleftharpoons CO_2 + H_2 \quad (6)$$

At typical SOFC operation conditions, reactions 1–5 are strongly limited by kinetics. The evaluation of conversion kinetics for just one decomposition phenomenon is difficult, as many reactions are simultaneously and consecutively occurring. Therefore, it is common to address kinetics for tar conversion by stating an overall rate of tar disappearance, where all reactions are lumped together [Herrmann, 2017].

Furthermore, it should be noted that higher hydrocarbons like naphthalene are more strongly adsorbed on the nickel catalyst than lower hydrocarbons. Hence, the reaction rate is perhaps best described as being proportional to the fraction of the covered surface. In that case, a kinetic approach like the Langmuir–Hinshelwood type can describe the conversion rate of tars [Speidel, 2016].

Concerning the potential effect of SOFC operating condition on the rate of carbon deposition when utilising tar-laden bio-syngas, Singh et al. [Singh, 2005] reported an in-depth thermodynamic analysis. It is based on the Gibbs free energy method, applied to an SOFC fed with a syngas comprising a mixture of toluene, naphthalene, phenol and pyrene, and considering the trend of the equilibrium concentration of 32 different species, including H_2, N_2, CO, CO_2, CH_4, H_2O and C(s). They obtained that the flow of a current through the cells avoids the possibility of C(s) formation. As the steam content in the fuel stream increases, the amount of C(s) is rapidly reduced to zero. The maximum rate of C(s) deposition is obtained at an operating temperature of 600°C, while it is lowest around 900°C.

Similar theoretical results have been obtained by Mermelstein et al. They stated, through a preliminary thermodynamic calculation that both current density and a S/C ratio > 1 are beneficial in mitigating carbon deposition coming from the presence of benzene in a H_2-N_2 mixture [Mermelstein, 2010]. Thermodynamic calculations suggested that operation temperatures above 750°C are unfavourable to

This project has received funding from the European Union's Horizon 2020 research and innovation programme under grant agreement No 815284

carbon deposition from syngas containing up to 15 g/Nm^3 of benzene.

Catalytic studies by Coll et al. show that for aromatic compounds the catalytic reactions leading to coke formation are faster than the rates of the reforming and carbon gasification reactions. The order of reactivity was benzene = toluene > anthracene > pyrene = naphthalene (see Figure 3). It was further shown that the mechanisms involved in coke deposition are catalytic, not pyrolytic, as the most favourable conditions were always at the lowest temperature. This indicates the high thermal stability of aromatic compounds [Coll, 2001].

Findings from Jess, who performed a catalytic study on the conversion of methane, benzene and naphthalene in H_2-H_2O, further indicate that the conversion of benzene and methane does not occur until naphthalene was completely consumed. This can be explained by the fact that naphthalene is strongly adsorbed on the nickel surface, decreasing the conversion of the other hydrocarbons. Once naphthalene was converted, yielding CO, H_2 and benzene, the weakly adsorbing benzene and methane were converted in a non-competitive fashion [Jess, 1996].

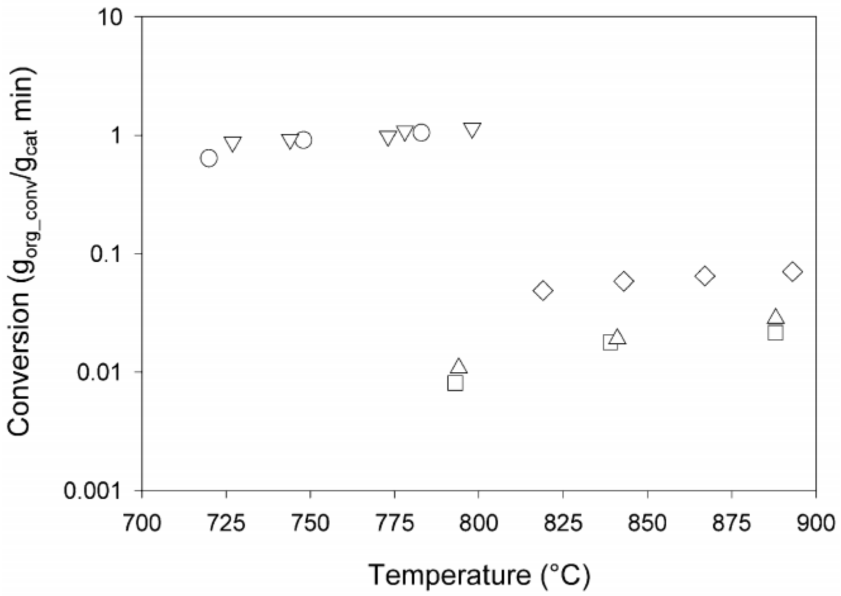

Figure 4. Comparison of conversion of toluene at S/C 3.8 (○), benzene at S/C 4.3 (▽), naphthalene at S/C 4.2 (□), anthracene at S/C 12.2 (◇), and pyrene at S/C 12.6 (△)against temperature [Coll, 2001].

Impact of tars on Ni-Zirconia Anode

With respect to experimental results obtained on SOFCs with Ni-YSZ or Ni-ScSZ anode on tar-laden fuels, the following information can be found in the open literature:

- Mermelstein reports about the operation of Ni-YSZ at 775°C with humidified hydrogen including 15 g/Nm3 benzene, toluene or a real tar mix. It concerned screen printed Ni-YSZ applied on a button cell [Mermelstein, 2009; Mermelstein, 2010].

- Hackett reports about the operation of Ni-YSZ at 800°C with a methane-free syngas and up to 150 ppm benzene. It concerned an anode-supported button cell.
- Lorente reports about the operation of Ni-YSZ at 765°C with humidified hydrogen including 15 g/Nm3 toluene or a real tar mix. It concerned screen printed Ni-YSZ applied on a button cell [Lorente, 2012; Lorente, 2013].
- Liu reports about the operation of Ni-YSZ at 800°C with syngas including 6.3 g/Nm^3 toluene. It concerned screen printed Ni-YSZ applied on a button cell [Liu, 2011].
- Namioka reports about the operation of Ni-ScSZ at 800°C with humidified hydrogen including toluene up to 50 g/Nm^3. It concerned screen printed Ni-ScSZ applied on a button cell [Namioka 2011; Namioka, 2012].
- Baldinelli reports about the operation of Ni-YSZ at 800°C with syngas including 10 g/Nm^3 toluene. It concerned an anode-supported button cell [Baldinelli, 2016].
- Pumiglia reports about the operation of Ni-YSZ at 650°C with syngas including up to 536 mg/Nm^3 toluene. It concerned an anode-supported button cell [Pumiglia, 2017].
- Geis and Jeong report about the operation of Ni-YSZ (both Ni-8SZ and Ni-3YSZ) at 700°C with syngas including phenol up to 8 g/Nm^3. In a recent publication, they also report about the operation of such cells under bio-syngas laden with a tar mix, both with and without the presence of sulphur. It concerned anode-supported cells with an active area of 81 cm^2 [Geis, 2016; Geis, 2018; Jeong, 2018].
- In a recent publication, Jeong also report about the operation of such cells under syngas including a tar mix, both with and without the presence of sulphur. It concerned a stack with anode-supported cells with an active area of 81 cm^2 [Jeong, 2019].
- Madi reports about the operation of Ni-YSZ at 800°C with humidified hydrogen or synthetic-bio-syngas including toluene up to 4350 ppm (22.8 g/Nm^3). It concerned an anode-supported cell with an active area of 8 cm^2 [Madi, 2015].
- Papurello reports about the operation of Ni-YSZ at 750°C with humidified hydrogen or synthetic bio-syngas including naphthalene up to 10 ppm (52 mg/Nm^3). It concerned a anode-supported button cell [Papurello, 2016].

Futhermore, there is literature available on the operation of alternative SOFC anode materials, predominantly Ni-GCO, either mentioned in comparative studies or from independent investigations. From these publications it has become clear that Ni-GCO is a better option for operation under hydrocarbon fuels due to the higher resistance to carbon formation. This is related to the properties of the catalyst support which, due to the improved oxygen ion mobility and electric conductivity, impedes the formation of carbon deposits in the anode microstructure. It should however be understood that it is the aim of the BLAZE project to demonstrate the feasibility of operation of a SOLIDpower stack under bio-syngas. This stack includes Ni-YSZ anode-supported cells and for this reason, a review of articles relevant for that aim deserve highest attention. Only in cases where results obtained with Ni-GCO have led to improved understanding on the carbon deposition phenomena, which otherwise should have been kept unmentioned, they are reported below.

Impact of tars present in hydrogen

Mermelstein et al. found from their investigations on benzene, toluene and a tar mix in dry hydrogen that toluene had the highest impact on the I-V behaviour of their SOFC with Ni-YSZ anode when the cells were operated at 765^{o}C, while benzene had the lowest impact. The anode exposed to 15 g/Nm^{3} tar mix had a performance between that of benzene and toluene. They further verified that thermal decomposition of benzene did not occur in their experimental set-up. The impedance spectra that they obtained are difficult to interpret due to large overlap in the polarization contributions and are therefore omitted here. Likely they were obtained at open circuit conditions, where results may be very different from those obtained under load. SEM-EDX observations on the tested anodes and nickel catalyst samples exposed to the tars indicate that both pyrolytic carbon and whisker carbon had formed with both model tars and the real tar mix but there appears to be an inconsistency to which extent coking occurred [Mermelstein, 2009]. In work from a year later they showed that even when steam is added, Ni-YSZ anode is prone to carbon deposition at 765^{o}C upon exposure to 15 g/Nm^{3} benzene in H_2 up to a S/C ratio of 3 [Mermelstein, 2010].

In a publication from Lorente et al, who followed the same experimental approach as Mermelstein, it was reported that nickel catalyst samples exposed for 30 minutes at 765^{o}C to 15 g/Nm^{3} toluene or real tar in hydrogen at a S/C ratio of 1 were both prone to carbon deposition, but toluene caused more carbon deposition than the real tar. TPO experiments revealed that the carbon resulting from real tar was more easily oxidised than carbon resulting from toluene [Lorente, 2012]. This seems to be in line with experiments from the same group reported a year later, where they exposed Ni-YSZ catalyst for 60 minutes at 765^{o}C to appr. 15 g/Nm^{3} tar fractions with different boiling points. It followed that carbon deposition was predominantly observed when the catalyst sample was exposed to the lightest tar fraction, and that this carbon was also more graphitic in nature, and that these lighter also have a greater propensity to form larger polyaromatic species and eventually graphitic carbon on the anode material [Lorente, 2013].

Namioka et al. have reported about the tolerance of Ni-YSZ anode operated at 800^{o}C and 0.5 A/cm^{2} current density. Over a period of 10 h, cells were exposed to different toluene concentrations ranging from 0 to 50 g/Nm^{3} in hydrogen at a S/C ratio of 1. SEM-EDX observations after testing revealed no

This project has received funding from the European Union's Horizon 2020 research and innovation programme under grant agreement No 815284

deposition of carbon until 10 g/Nm^3 toluene, while carbon deposition took place at tar loads of 20 and 50 g/Nm^3. In addition, it was observed that although the anode exposed to 10 g/Nm^3 toluene did not reveal carbon deposits, it did show an alteration of its free surface, indicating nickel depletion due to nickel dusting [Namioka, 2011]. In a publication from the same group one year later it followed that the problem of metal dusting was even more apparent than initially assumed. It was found that nickel dusting took place already at 3 g/Nm^3 toluene at 800^{o}C, which hardly improved when the operating temperature was increased to 900^{o}C. It also followed that the problem became more severe when the anode was kept at OCV while it became less apparent at increased S/C ratio, and thus that the severity of metal dusting was directly related to the amount of available steam [Namioka, 2012].

Madi et al. have reported about an anode-supported cell with Ni-YSZ anode operated at 750^{o}C and 0.25 A/cm^2 current density over a test period of 300 h under dry hydrogen including toluene op to a concentration of 7.3 g/Nm^3. They measured an impact of toluene on the cell voltage at a concentration of 3.6 g/Nm^3 and higher, with a dramatic drop in performance at the highest toluene concentration. Post mortem analysis revealed that central parts of the cell were damaged and that the nickel current collecting mesh had partially disintegrated, indicating metal dusting.

Papurello et al. have reported about the operation of an anode-supported cell with Ni-YSZ anode and 0.33 A/cm^2 current density over a test period of 7 h and measured no effect on the cell voltage up to a naphthalene concentration of 33 ppm. Post mortem results are not available because the cell was later on operated under syngas [Papurello, 2016].

Impact of tars present in syngas

Liu et al. performed tests on an SOFC with Ni-YSZ anode at 800^{o}C with syngas including 2.5-10% steam and 6.3 g/Nm^3 toluene. From thermodynamic calculations it followed that 2.5% steam would be sufficient to prevent carbon formation. Nevertheless the tests suffered from carbon deposits after operation for 5 h at 10% steam and 0.1 A/cm^2 current density. The interpretation of the impedance spectra obtained during the tests is confusing due to large overlap in the polarization contributions and is therefore omitted here [Liu, 2011].

Baldinelli et al. performed tests on an anode-supported SOFC with Ni-YSZ anode at 800^{o}C and 0.25 A/cm^2 current density with syngas with up to 10 g/Nm^3 toluene (total toluene exposure period 2 h). Thermodynamic calculations indicated carbon free conditions. Post mortem analysis revealed no carbon deposits, nor any other morphological changes compared with freshly reduced anode material.

In addition to their results obtained under tar laden hydrogen fuel, Madi et al. have reported about the operation of an anode-supported cell operated at 750^{o}C and 0.25 A/cm^2 current density with syngas

This project has received funding from the European Union's Horizon 2020 research and innovation programme under grant agreement No 815284

including up to 16 g/Nm^3 toluene. At low toluene concentrations of 1.7 g/Nm^3 and 5.6 g/Nm^3, no impact on the cell voltage was observed, but degradation occurred at 13.1 and 16 g/Nm^3. After the test, which altogether lasted 25 h, it was found that central parts of the cell were damaged and that the nickel current collecting mesh had partially disintegrated, indicating metal dusting [Madi, 2015].

Papurello et al. reported about the impact of toluene on the performance under syngas when using a Ni-YSZ anode-supported cell operated at 750°C. Substantial degradation was observed at 24 ppm toluene, most clearly being reflected in the low frequency polarization contribution related to mass transport and gas diffusion, while there was hardly an effect at 4 ppm toluene [Papurello, 2016].

Pumiglia et al. carried out tests on an anode-supported SOFC with Ni-YSZ anode at 650°C and 0.4 A/cm^2 with a methane-free bio-syngas and up to 0.53 g/Nm^3 toluene over a period of 150 h. In comparison to a cell that was operated under tar-free syngas, which operated stably, the cell with the tar-laden syngas degraded substantially. Post mortem analysis indicated deposition of carbon and, presumably as a result of pore clogging, local nickel oxidation. In addition, YSZ phase segregation and cracks were observed indication substantial mechanical stress during operation [Pumiglia, 2017].

The impact of benzene was investigated by Hackett et al. [Hackett, 2015]. From their tests, which were performed at 800°C at 0.25 A/cm^2 current density with a methane-free syngas, it follows that benzene has no negative effect on the cell voltage up to a concentration of 150 ppm over a test period of 500 h. Post mortem analysis revealed no presence of carbon, but clear changes in the nickel microstructure which authors speculated to be related to the formation of an amorphous solution of carbon with nickel.

Geis et al. performed tests on anode-supported cells with Ni-YSZ anode at 700°C and 0.34 A/cm^2 with syngas and up to 1.4 g/Nm^3 phenol. Total test time was 300 h. During the test, some degradation occurred but this could not unambiguously be related to the presence of phenol. Post mortem analysis revealed some carbon deposits between the anode-sided nickel current collecting mesh and the gold sensing wires, but no carbon was found on the anode itself. On the other hand, a spot was observed on the anode surface where the anode microstructure had changed. [Geis, 2016]. Further results followed in a publication from the year 2018. Here, a similar anode-supported cell was operated under comparable conditions but up to 8 g/Nm^3 phenol. At 4 g/Nm^3 phenol the cell started to exhibit voltage degradation, which became more aggravated when this was increased to 8 g/Nm^3 phenol. It was further observed that addition of phenol to the fuel stream caused voltage increase. Increased pressure drop over the housing at higher phenol loads indicated issues with the flow, likely due to carbon build-up. In addition, the results from three tests with an anode-supported cell with Ni-3YSZ anode were tested under comparable conditions and phenol loads of 0, 1.5 and 2.0 g/Nm^3, respectively. A voltage increase due to the presence of phenol was rarely observed during these tests. Voltage degradation was lower with the lower phenol load, but still higher than with clean syngas. After testing, the cells exposed to phenol indicated some carbon deposition adjacent to the anode nickel current collecting grid. In addition, substantial anode microstructural damage was observed in the fuel inlet manifold and in the fuel flow channels. Local detachment of the anode microstructure was observed, even for the lowest phenol concentration, which was speculated to be related with nickel dusting. All these degradation phenomena were not observed for the cell operated under clean syngas [Geis, 2018]. Deeper microstructure analyses on these cells, in particular those that were operated with 2.0 and 8 g/Nm^3 phenol, have been reported by Jeong et al. [Jeong, 2018]. This made clear that the local detachment of the anode microstructure triggered the formation of trenches in the anode support up to 150 microns deep, which appeared to be related to the local gas flow speed along the anode surface and thus the amount of tar that was in contact with the anode. In addition, a substantial increase of the substrate porosity and phase changes in the YSZ phase of the Ni-YSZ microstructure were observed, as well as the deposition of carbon fibers in the anode microstructures, the latter being more pronounced for the cell operated with 8 g/Nm^3 phenol, and up to a distance of 100 microns from the anode surface. As even in the case of 8 g/Nm^3 the formation of carbon deposits was expected based on thermodynamic calculations, it was finally hypothesised that reforming of phenol is at least partially triggered by substantial local cooling of the involved anode particles which would lead to conditions where solid carbon is more stable. Although metal dusting did not cause substantial degradation during the test, it is considered by be detrimental during long-term operation as the phenol progressively attacks the anode microstructure. No further explanation was given on the pressure drop build-up reported by Geis [Geis, 2018], and thus its exact cause is still an open question.

After finishing measurements under naphthalene-containing hydrogen gas, Papurello et al. investigated the impact of this tar component at 750°C up to concentrations of 10 ppm in syngas. Introduction of naphthalene caused voltage loss at concentrations as low as 1 ppm but then stabilised. This behaviour was seen up to 5 ppm. Higher concentrations were observed to cause a progressive decline in cell voltage, indicating considerable voltage loss upon prolonged operation. After removing naphthalene from the gas stream, the voltage recovered partially. It was further observed that adding naphthalene induced a drop in cell temperature, which the authors assumed to be related to inhibition of the (exothermic) water-gas shift reaction but additional tests under different fuel compositions confirmed that also the methane reforming reaction was inhibited [Papurello, 2016].

Further information about the impact of naphthalene on the operation of an anode-supported cell at 800°C and 0.25 A/cm^2 current density comes from the investigations by Hacket et al., who performed tests under methane-free syngas [Hackett, 2015]. Compared with operation under tar-free syngas, the initial performance under naphthalene-bearing fuel was lower (kept unaddressed by authors) while the degradation rate was higher. While at 100 pm naphthalene the voltage decline was limited, a clear

This project has received funding from the European Union's Horizon 2020 research and innovation programme under grant agreement No 815284

increase of the polarization resistance at 1000 Hz was observed. At 500 ppm naphthalene the voltage decline was larger, and in this case the impedance spectroscopy data indicated predominantly an increase of the polarization resistance at 100 Hz. As for the tests performed under benzene containing syngas, post mortem analysis revealed no presence of carbon, but clear changes in the nickel microstructure was observed after exposure to naphthalene, which the authors speculated to be related to the formation of an amorphous solution of carbon with nickel.

In a recent publication from Jeong et al. the results are reported from a 4-cell stack test with Ni-3YSZ anode supported cells at 715^{o}C connected to a gasifier with additional deep tar cleaning. While stable performance was obtained under tar free gasifier-gas the performance under tar-laden gas (total tar load 3.5 g/Nm^3) was problematic, the fuel cell experienced a rapid increase of the pressure drop over a time period of 5 hours, while a comparative test where deep tar cleaning was maintained did not show this problem. Post mortem analysis revealed heavy carbon deposition on all four cells of the tar-exposed stack, in particular at the fuel inlet manifold, the cell inlet and on the nickel current collecting mesh at the fuel inlet, indicating that the tars were responsible for the carbon. SEM-EDX revealed that the carbon on the anode was mostly present in the form of fibers, often with a nickel particle on the fiber tip, while carbon deposited on the nickel mesh was more disordered, indicating an influence of the nickel particle size on the carbon morphology. In addition, nickel coarsing was observed while the YSZ present in the anode microstructure remained intact [Jeong, 2019].

4.4 Exposure to sulphur

Sulphur has long been known for its deleterious effects on the SOFC performance. The first who systematically investigated the impact of sulphur on the electrochemical performance were Matsuzaki et al [Matsuzaki, 2000]. In this work it was reported that the poisoning effect with 0.05 to 2 ppm H_2S in hydrogen fuel was dependent on temperature, the equilibrium partial pressure of sulphur and the total sulphur concentration in the fuel. The time needed to achieve a metastable cell voltage after sulphur poisoning was almost independent of the sulphide concentration and was found to increase with decreasing temperature. The authors suggested that the poisoning that they observed was most likely related to an adsorption effect. This was later confirmed by Rasmussen and Hagen, who carried out in-plane voltage measurements on an SOFC while sulphur was introduced in the fuel stream and upon recovery, and found that the sulphur poisoning effect was well related to the local gas composition which could only be explained by a fast chemisorption effect [Rasmussen, 2009]. Similar observations were made by Blesznowksi et al [Blesznowksi, 2013].

It was further found that at increased sulphur concentration irreversible effects were also possible. In this case, the poisoning consisted of at least two stages, i.e. a reversible initial voltage drop within a few minutes to a metastable cell voltage, followed by gradual and irreversible voltage degradation, which was sometimes followed by fatal performance loss. Sasaki et al. measured irreversible sulphur poisoning at 5 ppm H_2S in H_2 or H_2-CO, depending on temperature and fuel composition [Sasaki, 2006]. Zha et al. carried out tests with fuel including 2 and 50 ppm H_2S and measured a fast drop in cell performance in the first several minutes, followed by a slow but continuous drop in the next 120 h. The sulphur poisoning effect was accumulative and became more severe with increasing H_2S concentration [Zha, 2007]. Similar observations were made by Hagen [Hagen, 2013]. Norheim et al. also measured a voltage decline upon introducing H_2S in the fuel stream but did not measure irreversible degradation, but this was perhaps related to the short exposure time [Norheim, 2007].

Besides the poisoning effect of sulphur on the electrochemical oxidation of hydrogen, its impact on the activity of nickel for the water-gas shift reaction and the direct steam reforming of hydrocarbons has been investigated. At 750°C, the addition of 1 ppm H_2S to CO/H_2O fuel led to a complete poisoning of the WGS reaction and a subsequent lack of hydrogen for the electrochemical reaction, while the remaining CO was not electrochemically converted [He, 2008]. Kromp et al. revealed that already at 0.5 ppm H_2S, the sulphur poisoned the WGS reaction which inhibited conversion of CO within the fuel [Kromp, 2012]. Hagen experienced considerable voltage loss at 2 ppm H_2S in $CO/H_2/H_2O$ fuel at 850°C and 0.5 A/cm^2 current density and, after increasing to 8 ppm H_2S, only partial recovery. Similar observations were made at 750°C and 0.25 A/cm^2. As the observed tolerance to H_2S was lower than in the case of H_2-H_2O fuel, it was concluded that the WGS reaction was inhibited [Hagen, 2013]. Li et al., who performed tests on Ni-YSZ anode operated at 800°C in humidified syngas with and without the presence of 2 ppm H_2S, on the other hand, showed by means of exhaust gas analysis, that CO was still converted in the presence of sulphur. Authors suggest that this could be related to the presence of steam [Li, 2014]. An impedance study by Weber et al. on Ni-YSZ anode operated at 750°C revealed detailed information about the impact of sulphur on the anode processes, from which it follows that sulphur poisoning in H_2/H_2O mixture causes an increase of the polarization contributions at appr. 3 kHz and 100 Hz, which authors relate to poisoning of active triple phase boundaries in the electrochemically active part of the anode, while poisoning in the presence of methane-free syngas additionally causes an increase of the polarization contributions at 10 Hz and 1 Hz, the latter of which is ascribed to CO/CO_2 diffusion, and thus indicating inhibition of the WGS reaction. By comparing the temporal characteristics of the polarization resistance of two different anode supported cells, it was further shown that the accumulated H_2S-amount divided by the available Ni-surface area determine the onset of the degradation [Weber, 2013].

The first indications that the impact of sulphur impacts the reforming of CH_4 were reported by Bartholomew et al. [Barthomolew, 1982]. Similar effects were reported by Rostrup-Nielsen [Rostrup-Nielsen, 2006], Smith [Smith, 2009], Hagen et al. [Hagen, 2011] and Li et al. [Li, 2014]. Hagen et al. showed that in the presence of significant amounts of CH_4, Ni-YSZ anode is severely poisoned at concentrations of 2 ppm H_2S at 850°C, experiencing a partly irreversible loss due to a loss of percolation of Ni particles close the electrolyte [Hagen, 2011]. Further mechanistic explanations on how sulphur interacts with nickel in relation to methane reforming can be found in a paper from Kuhn et al. [Kuhn, 2008].

The most likely reason behind the dramatic impact of sulphur on the catalytic activity of nickel at low sulphur concentrations appears to be the isosteric heat of adsorption for H_2S on nickel, which value is much higher than the heat of formation for bulk nickel sulphide. In other words: the low sticking effect of H_2S on nickel allows the H_2S to quickly reach the anode/electrolyte interface, where it will adsorb on nickel, hinder the adsorption of other active species and thereby the electrochemical oxidation of hydrogen [Gong, 2007]. Hansen was the first to relate the sulphur coverage of nickel with the impact of sulphur on the electrochemical performance [Hansen, 2008]. He did this by using a Temkin isotherm, by which the sulphur coverage was successfully related to the performance drop for Ni-YSZ anodes reported in previous literature.

The irreversible performance drop caused by sulphur was less easy to explain. Some research groups associated it with the agglomeration of Ni particles due to the formation of nickel sulphides [Sasaki, 2006; Dong, 2005; Dong, 2006; Braun, 2008; Cheng, 2007; Mougin, 2007]. Alternatively, it has been proposed that the adsorbed sulphur species could lead to surface reconstruction of the nickel particles without the formation of secondary phases [Rasmussen, 2009; Oliphant, 1978]. Such an effect is expected to be much slower than the surface adsorption process and may cause a much slower degradation in fuel cell performance by changing the exposed crystal planes to less active ones [Zha, 2007]. The answer seems to follow from work by Li et al., who exposed Ni-YSZ anode at 800°C to both dry and humidified hydrogen fuel in the presence of 0.2% H_2S. They found that Ni-YSZ anode operated in dry conditions caused the formation of small nickel sulphide dots on the nickel particles, whereas in presence of 3-10% steam, which alleviated the poisoning effect, these nickel sulphide dots were less clearly visible [Li, 2011]. The trigger for alteration of the anode microstructure due to sintering, which might be more detrimental than dissolution of sulphur in the nickel bulk, was later suggested to be the result of combined attack of the nickel particles by sulphur and oxygen, the latter of which being the result of high anode overpotential [Hauch, 2014].

In addition, it might be that the nature of the oxide that is mixed with nickel to form the anode cermet is important [Sasaki, 2006]. It is assumed that oxygen spillover from the oxide to the nickel helps to prevent permanent nickel deactivation. Such an effect would become more pronounced as the oxygen ion conductivity of the oxide increases or when the physical contact between the cermet particles becomes more intimate.

It has further been proposed that the presence of sulphur may reduce the risk of coking as the nickel, either because sulphur preferentially binds to the nickel sites that are most active for coke formation and steam reforming which leaves only the less active (terrace) sites available for reforming, and these are less prone to coking, or occupying part of the nickel atoms on the highly active sites, or by incorporation of sulphur in the nickel lattice [Kuhn, 2008]. The downside of all this is that the sulphur potentially deactivates the nickel sites for the electrochemical oxidation of hydrogen and up to now, there is no indication that this can be selectively prevented.

4.5 Exposure to halogens

Chlorine is typically present in the form of HCl in bio-syngas. Li et al. studied the impact of 8 ppm HCl at 850^{o}C and 10 ppm HCl at 750^{o}C during 1 h tests in hydrogen and found no observable effect. [Li, 2010]. Blesznowksi et al. found that 3 ppm HCl in the feed did not cause degradation for 48 hr tests, while 10 ppm HCl in the feed caused a recoverable voltage drop of only 10 mV during a 67 h test [Blesznowski, 2013]. Encouraging results also from Bao [Bao, 2009] and Buchinger [Buchinger, 2006], who found no observable degradation due to the presence of 40 and 47 ppm HCl, respectively. Marina et al. tested their Ni-YSZ anodes in the presence of 800 ppm HCl and measured a recoverable voltage loss [Marina, 2010]. The mechanism of poisoning by chlorine is suggested to involve adsorption of chlorine on the nickel surface, but information about the long-term stability is limited, and thus calls for further investigation.

4.6 Exposure to alkali metals

Only little information is available on the influence of alkali metals on the SOFC. Up to the author's knowledge, only Nurk et al. and Mougin et al. have published about its long-term effects, by exposing an SOFC with Ni-GDC anode to H_2-N_2-H_2O fuel including up KCl, thus investigating the impact of potassium representing alkali metals together with that of chlorine. For the evaporation of KCl a special salt evaporation and condensation system was developed, which allowed for producing salt vapours with known concentration and feeding these in a controlled way to the SOFC. A long term test at 900^{o}C including 6 ppm KCl revealed no performance decay over a test period, while a test including 3500 ppm resulted in a fast increase of the polarisation resistance as well as the ohmic losses. Post mortem analysis showed that at low concentrations the KCl preferentially deposited on the surface of the SOFC anode. The loss in performance that was observed at 3500 ppm KCl was tentatively ascribe to a blocking of pores inside the SOFC anode [Nurk, 2009]. The results reported by Mougin et al. reported on the exposure to 100 ppm KCl indicated the presence of potassium on the anode surface, but the results are insufficient to make any further statements about the long term effects on anode microstructure and SOFC electrochemical performance [Mougin, 2007].

This project has received funding from the European Union's Horizon 2020 research and innovation programme under grant agreement No 815284

5 RECOMMENDATIONS

Based on the above literature, it can be concluded that, although SOFCs in comparison to other fuel cell types are quite fuel tolerant, integration of an SOFC with a BFB steam gasifier has to be done with care.

With respect to the main constituents in the bio-syngas after high temperature gas cleaning it can be assumed that the gas is at thermodynamic equilibrium. However, depending on the additional clean-up that might need to be integrated prior to feeding the gas to the SOFC, some intermediate cooling has to be considered. In order to assess if the lower temperatures may give rise to carbon formation in the BoP, it is recommended to perform additional thermodynamic calculations.

Although it is expected that with proper tar cleaning, low tar levels (below 0.5 g/Nm^3) can be obtained, the tars deserve high attention. It follows that most, if not all tar compounds are stable enough to avoid the formation of pyrolytic carbon due to thermal cracking, they will give rise to carbon formation once they have come in contact with the nickel particles that exist in the SOFC anodes. Also in this case, a first approximation for the extent of carbon formation may come from thermodynamic calculations, but in addition the slow kinetics in the conversion of the tar compounds on the surface of the nickel particles should be considered. In particular, naphthalene and pyrene are tedious compounds with slow conversion kinetics, and consequently accumulate easily in the SOFC anodes. In addition, it has been suggested that due to the strong endothermic nature of the (complex) tar conversion reactions, the local conditions may be very different from what one may assume from the readings. Generally speaking, it can be stated that higher operating temperatures will alleviate the carbon deposition issue. To a small extent this may be realised during the final demonstration, where a maximum operating temperature of the SOFC stack of 790^{o}C is tolerated. But even in cases where carbon deposits after testing are not apparent, it might happen that due to the slow kinetics for tar conversion, the SOFC may experience degradation due to metal dusting, damaging the anode microstructure and nickel mesh, and thus limit the operational lifetime of the system.

It has been shown that tars as well as sulphur poison catalytically and electrochemically active sites in the SOFC anode, which limits the conversion of other fuel constituents such as H_2, CO and CH_4. Among these, the conversion of CO and CH_4 appear to be affected the most, the first because the WGS reaction is inhibited, the latter because the steam reforming reaction is inhibited. The electrochemical oxidation of hydrogen seems the least affected, so it might be worth to consider gasification conditions that limit the concentrations of CO and CH_4 while optimizing the H_2 yield. For sulphur, the poisoning effect is likely the adsorption of sulphur on the nickel surface or nickel surface modification due to reaction with sulphides. At higher sulphur concentrations, irreversible damage may also result, depending on the anode microstructure, gas composition, sulphur load and exposure time, and the local operating conditions.

This project has received funding from the European Union's Horizon 2020 research and innovation programme under grant agreement No 815284

With respect to other contaminants that might arrive from the gasifier, it appears that HCl and alkali metals are less problematic than tars or sulphur, but the amount of available literature is limited. Likewise, it is difficult to give limits for the contaminant levels for the SOFC stack. Although there is literature available that describes the impact of tars and sulphur, most of the experiments were done on small samples for limited time, and it is thus unclear how this will affect the performance and longevity of the considered SOFC stack, given its operating conditions (temperature, fuel utilization, etc.) in relation the properties of the SOFC Ni-YSZ anode. This calls for further experimental work, where detailed understanding about the impact on the SOFC anode is obtained, using the latest techniques such as impedance spectroscopy, as well as detailed post mortem analysis, also with the latest techniques. Something that deserves particular attention in this respect are the synergetic or counteracting effects of contaminants.

Taking all of the above into consideration, the following experimental approach is suggested for WP 3:

- In order to prevent carbon deposition the main gas composition should allow for cooling to 450°C in case desulphurization needs to take place with ZnO. According to the publication from Savuto et al. this should be possible for syngas obtained at a steam-to-biomass ratio of 0.5 (see also Figure 1). Thus, it is suggested to use the following syngas composition on wet basis: 45% H_2, 24% CO, 11% CO_2, 2% CH_4, 18% H_2O.
- Naphthalene has been selected to represent so-called slow tars, i.e. tars with slow conversion kinetics. In order to make meaningful tests, the investigated contaminant levels will be aligned with those reported in literature regarding experimental work on SOFCs, i.e. 25 mg/Nm^3 (5 ppm) and 75 mg/Nm^3 (15 ppm) naphthalene.
- Toluene has been selected to represent so-called fast tars, i.e. tars with relatively fast conversion kinetics. Tolerable toluene levels are less clear than for naphthalene, and thus will be aligned with those expected from BFB steam gasifiers with catalytic filters, i.e. 250 mg/Nm^3 (to be expected from clean biomass such as almond shells) and 750 mg/Nm^3 (feedstock emitting high toluene concentrations).
- H_2S has been selected to represent sulphur compounds. In order to make meaningful tests, the investigated contaminant levels will be aligned with those reported in literature regarding experimental work on SOFCs, i.e. 1 ppm and 3 ppm H_2S.
- KCl has been selected to represent both halogens and alkalis. Although it is unclear whether KCl will actually reach the SOFC in this form, other compounds like HCl and alkali hydroxides might reach the SOFC, and therefore investigating the impact of halogens and alkalis is relevant. Thus, KCl is considered a suitable representative to simultaneously assess the impact of halogens and alkali metals. Investigated contaminant levels are 50 ppm and 200 ppm KCl.

This project has received funding from the European Union's Horizon 2020 research and innovation programme under grant agreement No 815284

Further details about the experimental approach will be addressed in separate deliverables under responsibility of ENEA and EPFL, respectively.

6 CONCLUSIONS

Based on the literature that has been reviewed in order to assess the feasibility of connecting an SOFC to a bubbled fluidised bed steam gasifier, it can be concluded that the longevity of the SOFC is likely to be at risk if no further gas cleaning will take place. Particularly problematic gas compounds are tars, sulphur, halogens (in particular chlorine), and alkali metals (in particular sodium and potassium). This calls for careful assessment of the SOFC tolerance limits where prolonged operation without substantial degradation is still possible, which will be carried out in work package 3, as well as the investigation of additional gas cleaning, which will be addressed in work package 2. Preferably, the additional gas cleaning takes place at high temperature, as this will simplify the integration of the SOFC with the gasifier. In case intermediate cooling is required to sufficiently clean the bio-syngas, it should be checked that the gas oxygen-to-carbon ratio is sufficiently high to avoid carbon deposition following thermodynamic calculations, and that contaminants will not condense out in a detrimental way.

The experimental work that will be performed in work package 3 will aim to determine the tolerance levels for naphthalene, which will represent tars with low conversion kinetics, toluene, which will represent tars with relatively high conversion kinetics, H_2S, which is the main sulphur species, and KCl, which represents both halogen compounds and alkali metals that could arrive in various forms from the gasifier.

7 REFERENCES

1. [Alstrup, 1998] I. Alstrup, M.T. Tavares, C.A. Bernardo, O. Sørensen, J. Rostrup-Nielsen, Mat. and Corr., 49 (1998) 367
2. [Aravind, 2012] P.V. Aravind, W. de Jong, Progr. in En. And Comb. Sci. 38 (2012) 737
3. [Baker, 1975 (1)] R.T.K. Baker, P.S. Harris, J. Henderson, R.B. Thomas, Carbon, 1975, 13, 37.
4. [Baker, 1975 (2)] R.T.K. Baker, P.S. Harris, S. Terry, Nature, 1975, 253, 37.
5. [Baker, 1989] R.T.K. Baker, Carbon, 1989, 27, 315.
6. [Baldinelli, 2016] A. Baldinelli, G. Cinti, U. Desideri, F. Fantozzi, En. Conv. Man. 128 (2016) 361
7. [Bao, 2009] J. Bao, G.N. Krishnan, P. Jayaweera, K.-H. Lau, A. Sanjurjo, J. Power Sources 193 (2009) 617
8. [Bartholomew, 1982] C.H. Bartholomew, Catal Rev 24 (1982) 112
9. [Blesznowski, 2013] M. Blesznowski, J. Jewulski, A. Zieleniak, Centr. Eur. J. Chem., 11 (2013) 960
10. [Buchinger, 2006] G. Buchinger, P. Hinterreiter, T. Raab, S. Griesser, J. Fuel Cell Sci. and Techn. 3 (2006) 280
11. [Campoy, 2014] M. Campoy, A. Gómez-barea, P. Ollero, S. Nilsson, Fuel Proc. Tech. 121 (2014) 63-69
12. [Canova, 1993] J.H. Canova, D.J. Bushnell: Testing and evaluating the combustion characteristics of densified RDF and mixed waste paper. In: Proc. Energy from biomass and wastes XVI (Ed. D.L.Klass), pp. 1191-1219, Institute of Gas Technology, Chicago (1993).
13. [Coll, 2001] R. Coll, J. Salvado, X. Farriol, D. Montane, Fuel Proc. Tech. 74 (2001) 19
14. [D'Orazio 2015] A. D'Orazio, S. Rapagnà, P.U. Foscolo, K. Gallucci, M. Nacken, S. Heidenreich, A. Di Carlo, A. Dell'Era, Int. J. Hydrog. Energy 40 (2015) 7282–7290
15. [Devi, 2005] L. Devi, K.J. Ptasinski, F.J.J.G. Janssen, S.V.B. van Paasen, P.C.A. Bergman, J.H.A. Kiel, Ren. En. 30 (2005) 565
16. [Geis, 2016] M. Geis, S. Herrmann, S. Fendt, H. Spliethof, 12th European SOFC & SOE Forum, Lucerne, 5-8 July 2016, 160
17. [Geis, 2018] M. Geis, S. Herrmann, S. Fendt, H. Jeong, C. Lenser, N.H. Menzler, H. Spliethof, Int. J. Hydr. En. 43 (2018) 20417
18. [Gong, 2007] M. Gong, X. Liu, J. Trembly, C. Johnson, J. Power Sources 168 (2007) 289
19. [Hackett, 2015] G.A. Hackett, K. Gerdes, Y, Chen, X. Song, J. Zondlo, Met. Mat. Trans. 58 (2015) 58
20. [Hagen, 2011] A. Hagen, J.F.B. Rasmussen, K. Thyden, J. Power Sources 196 (2011) 7271
21. [Hagen, 2013] A. Hagen, J. Electrochem. Soc. 160 (2013) F111
22. [Hansen, 2008] J.B. Hansen, Electrochem and Solid-State Lett. 11 (2008) B178
23. [Hauch, 2014] A. Hauch, A. Hagen, J. Hjelm, T. Ramos, J. Electrochem. Soc. 161 (2014) F734
24. [He, 2008] H.P. He, A. Wood, D. Steedman, M. Tilleman, Solid State Ionics 179 (2008) 1478
25. [Heidenreich, 2013] S. Heidenreich, Fuel 104 (2013) 83-94
26. [Herrmann, 2017] T. Herrmann, M. Dillig, M. Hauth, J. Karl, En. Sci. Eng. 5 (2017) 194
27. [Holstein, 1995] W.L. Holstein, J. Cat., 1995, 152, 42
28. [Horita, 2004 (1)] T. Horita, K. Yamaji, T. Kato, N. Sakai, H. Yokokawa, J. Power Sources 131 (2004) 299
29. [Horita, 2004 (2)] T. Horita, K. Yamaji, T. Kato, N. Sakai, H. Yokokawa, Solid St. Ionics 172 (2004) 93

30. [Jeong, 2018] H. Jeong, M. Geis, C. Lense,r S. Lobe, S. Herrmann, S. Fendt, N.H. Menzler, O. Guillon, Int. J. Hyrd. En. 43 (2018) 20911
31. [Jeong, 2019] H. Jeong, M. Hauser, F. Fischer, M. Hauck, S. Lobe, R. Peters, C. Lenser, N.H. Menzler, O. Guillon, J. Electrochem. Soc. 166 (2019) F137
32. [Jess, 1996] A. Jess, Chem. Eng. Proc. 35 (1996) 487
33. [Kinoshita, 1994] C.M. Kinoshita, Y. Wang, J. Zhou, J. Anal. Appl. Pyrolysis 29 (1994) 169
34. [Keep, 1977] C.W. Keep, R.T.K. Baker, J.A. France, J. Catal., 1977, 47, 232.
35. [Kim, 2001] H. Kim, S. Park, J.M. Vohs, R.J. Gorte, J. Electrochem. Soc. 148 (2001) A693
36. [Kishimoto, 2004] H. Kishimoto, T. Horita, K. Yamaji, Y. Xiong, N. Sakai, H. Yokokawa, Solid St. Ionics 175 (2004) 107
37. [Kishimoto, 2007] H. Kishimoto, K. Yamaji, T. Horita, Y. Xiong, N. Sakai, M.E. Brito, H. Yokokawa, J. Power Sources 172 (2007) 67
38. [Kromp, 2012] A. Kromp, S. Dierickx, A. Leonide, A. Weber, E. Ivers-Tiffee, ECS Transactions 41 (2012) 161
39. [Kuhn, 2008] J.N. Kuhn, N. Lakshminarayanan, U.S. Ozkan, J. Mol. Cat. A: Chem. 282 (2008) 9
40. [Li, 2010] T.S. Li, W.G. Wang, H. Miao, T. Chen, C. Xu, J. Alloys Compd. 495 (2010) 138
41. [Li, 2011] T.S. Li, W.G. Wang, J. Power Sources 196 (2011) 2066
42. [Li, 2014] T.S. Li, M. Xu, C. Gao, B. Wang, X. Liu, B. Li, W.G. Wang, J. Power Sources 258 (2014) 1
43. [Lin, 2006] Y. Lin, Z. Zhan, S.A. Barnett, J. Power Sources 158 (2006) 1313
44. [Liu, 2011] M. Liu, M.G. Millan, P.V. Aravind, N. Brandon, J. Electrochem. Soc. 158 (2011) B1310
45. [Lorente, 2012] E. Lorente, M. Millan, N.P. Brandon, Int. J. Hydr. En. 37 (2012) 7271
46. [Lorente, 2013] E. Lorente, C. Berrueco, M. Millan, N.P. Brandon, J. Power Sources 242 (2013) 824
47. [Madi, 2015] H. Madi, S. Diethelm, C. Ludwig, J. Van Herle, ECS Transactions 68 (2015) 2811
48. [Marina, 2010] O.A. Marina, L.R. Pederson, E.C. Thomsen, C.A. Coyle, J. Power Sources 195 (2010) 7033
49. [Matsuzaki, 2000] Y. Matsuzaki, I. Yasuda, Solid State Ionics 132 (2000) 261
50. [Mermelstein, 2009] J. Mermelstein, M. Millan, N.P. Brandon, Chem. Eng. Sci. 64 (2009) 492
51. [Mermelstein, 2010] J. Mermelstein, M. Millan, N. Brandon, J. Power Sources 195 (2010) 1657
52. [Mogensen, 2011] D. Mogensen, J.D. Grunwaldt, P.V. Hendriksen, K. Dam-Johansen, J.U. Nielsen, J. Power Sources 196 (2011) 25
53. [Monnerat, 2001] B. Monnerat, L. Kiwi-Minsker, A. Renken, Chem. Eng. Sci., 2001, 56, 633.
54. [Mougin, 2007] J. Mougin, S. Ravel, E. De Vito, M. Petitjean, ECS Transactions 7(1) 459-468 (2007)
55. [Nacken 2015] M. Nacken, G.V. Baron, S. Heidenreich, S. Rapagnà, A. D'Orazio, K. Gallucci, J.F.M. Denayer, P.U. Foscolo, Fuel Process. Technol. 134 (2015) 98–106,
56. [Namioka, 2011] T. Namioka, T. Naruse, R. Yamane, Int. J. Hydr. En. 36 (2011) 5581
57. [Namioka, 2012] T. Namioka, Y. Nagai, K. Yoshikawa, T. Min, Int. J. Hydr. En. 37 (2012) 17245
58. [Nguyen, 2016] H.N.T. Nguyen, N. Berguerand, G.L. Schwebel, H. Thunman, Ind. Eng. Chem. Res. 55 (2016) 11900
59. [Norheim, 2007] A. Norheim, I. Waernhus, M. Brostrom, J.E. Hustad, A. Vik, Energy & Fuels 21 (2007) 1098
60. [Nurk, 2009] G. Nurk, A. Kubacki, L. Holzer, R. Figi, T. Graule, P. Holtappels, ECS Transactions 25 (2) 2117-2124 (2009)

This project has received funding from the European Union's Horizon 2020 research and innovation programme under grant agreement No 815284

61. [Pallozzi, 2018] V Pallozzi, A. Di Carlo, E. Bossci, M. Carline, Biomass and Bioeneergy 109 (2018) 85-90
62. [Papurello, 2016] D. Papurello, A. Lanzini, P. Leone, M. Santarelli, Ren. En. 99 (2016) 747
63. [Pumiglia, 2017] D. Pumiglia, S. Vaccaro, A. Masi, S.J. McPhail, M. Faconieri, S. Gagliardi, L. Della Seta, M. Carlini, J. Power Sources 340 (2017) 150
64. [Rakesh, 2018] N. Rakesh, S. Dasappa, Ren. And Sust. En. Reviews 91 (2018) 1045
65. [Rapagnà 2010] S. Rapagnà, K. Gallucci, M. Di Marcello, M. Matt, M. Nacken, S. Heidenreich, P.U. Foscolo, Bioresour. Technol. 101 (2010) 7123–7130.
66. [Rapagnà 2012] S. Rapagnà, K. Gallucci, M. Di Marcello, P.U. Foscolo, M. Nacken, S. Heidenreich, M. Matt, Fuel. 97 (2012) 718–724.
67. [Rapagnà, 2018] S. Rapagnà, K. Gallucci, P.U. Foscolo, Waste Management 71 (2018) 792-800
68. [Rasmussen, 2009] J.F.B. Rasmussen, A. Hagen, J. Power Sources 191 (2009) 534
69. [Rostrup-Nielsen, 2006] J.R. Rostrup-Nielsen, J.B. Hansen, S. Helveg, N. Christiansen, A.-K. Jannasch, Appl. Phys. A 85 (2006) 427
70. [Sasaki, 2006] K. Sasaki, K. Susuki, A. Iyoshi, M. Uchimura, N. Imamura, H. Kusaba, Y. Teraoka, H. Fuchino, K. Tsujimoto, Y. Uchida, N. Jingo J. Electrochem. Soc. 153 (2006) A2023
71. [Saunders, 2004] G.J. Saunders, J. Preece, K. Kendall, J. Power Sources 131 (2004) 23
72. [Savuto, 2019] E. Savuto, A. Di Carlo, A. Steele, S. Heidenreich, K. Gallucci, S. Rapagna, Fuel Processing Technology 191 (2019) 44
73. [Singh, 2005] D. Singh, E. Hernandez-Pacheco, P.N. Hutton, N. Patel, M.D. Mann, J. Power Sources 142 (2005) 194
74. [Smith, 2009] T.R. Smith, A. Wood, V.L. Birss, Appl. Cat. A: Gen. 354 (2009) 1
75. [Stemmler, 2013 (1)] M. Stemmler, A. Tamburro, M. Müller, Biomass Conv. Bioref. (2013) 3:187-198
76. [Stemmler, 2013 (2)] M. Stemmler, A. Tamburro, M. Müller, Fuel 108 (2013) 31-36
77. [Stevens, 2001] J.D. Stevens, NREL/SR-510-29952, National Renewable Energy Laboratory, Golden, Colorado
78. [Szakalos, 2004] P. Szakalos, Doctoral Thesis, Royal Institute of Technology, Stockholm, Sweden.
79. [Timmermann, 2007] H. Timmermann, W. Sawady, D. Campbell, A. Weber, R. Reimert, E.Ivers-Tiffee, ECS Transactions 7 (2007) 1429
80. [Toh, 2003] C.H. Toh, P.R. Munroe, D.J. Young, K. Foger, Mater. High Temp., 2003, 20, 129.
81. [Trimm, 1977] D.L. Trimm, Catal. Rev. 16 (1977) 155
82. [Ud Din, 2016] Z. Ud Din, Z.A. Zainal, Ren. And Sust. En. Reviews 53 (2016) 1356
83. [Weber, 2013] A. Weber, S. Dierickx, A. Kromp, E. Ivers-Tiffee, Fuel Cells 13 (2013) 487
84. [Wilk, 2013] V. Wilk, H. Hofbauer, Energy & Fuels 2013, 27, 3261-3273
85. [Yamaji, 2006] K. Yamaji, H. Kishimoto, Y. Xiong, T. Horita, N. Sakai, M.E. Brito, H. Yokokawa, J. Power Sources 159 (2006) 885
86. [Yamaji, 2008] K.Yamaji, H. Kishimoto, Y. Xiong, T. Horita, N. Sakai, M.E. Brito, H. Yokokawa, Solid St. Ionics 179 (2008) 1526
87. [Young, 2009] D. Young, J. Zhang, ECS Trans. 44 (2009) 3
88. [Zha, 2007] S. Zha, Z.Cheng, M.Lui, J. Electrochem. Soc. 154 (2007) B201